(Received 6 January 2026, Accepted 5 March 2026, Scheduled 6 April 2026)

Investigations on Circular Slot Ring Structured Antenna for Triple Band Frequencies and UWB Applications

P. Sushma Chowdary[1], K. Radha[2], Ravi Kumar Maddumala[2], B. Ajay Kumar[3], and Bokkisam Venkata Sai Sailaja[4,*]

[1]*Department of Electronics and Instrumentation Engineering, Siddhartha Academy of Higher Education, deemed to be University Vijayawada-7, Andhra Pradesh, India*
[2]*Department of Electronics and Communication Engineering, Sir CR Reddy College of Engineering Eluru, Andhra Pradesh 534007, India*
[3]*Department of Electronics and Communication Engineering, SR Gudlavalleru Engineering College Vijayawada, Andhra Pradesh 521356, India*
[4]*Department of Electronics and Communication Engineering, KLEF (deemed to be University) Vaddeswaram, Guntur-522502, India*

ABSTRACT: In this paper, we present a microstrip feed slot ring resonator with a central circular disc antenna that operates at triple bands. The suggested antenna covers 5G, military, radar, and UWB applications. It resonates within 2.71 GHz–12 GHz at center frequencies of 4.13 GHz ($S_{11} = -17.9$ dB), 8.53 GHz ($S_{11} = -38$ dB), and 9.09 GHz ($S_{11} = -20$ dB). Simulations of the ultra-wideband antenna matched the manufactured devices. The proposed antenna has dimensions of $40 \times 42 \times 1.6\,\text{mm}^3$ and is constructed on a cost-effective FR4 substrate. It achieves an operating impedance of less than -10 dB. The circular ring slot antenna shows remarkable capabilities, achieving multiband frequencies at 4.13 GHz, 8.53 GHz, and 9.09 GHz. The unique ultra-wideband design has a positive impact on gain and yields stable radiation characteristics, with surface currents contributing to a promising design. The design achieves a gain of about 5 dBi and a fractional bandwidth of roughly 128.7%.

1. INTRODUCTION

The rapid development of 5G and upcoming wireless technologies has significantly shaped antenna research. Current communication systems require antennas that are compact, support multiple bands with stable radiation, and have lightweight structures suitable for integration with miniaturized systems. As a result, research trends focus on three major directions: miniaturization, multi-band/wideband operation, and novel materials or configurations for enhanced efficiency. These trends have driven engineers to explore new materials, design methodologies, and advanced structures to improve bandwidth and efficiency, as reflected in recent literature.

In [1], a flexible moon-inspired coplanar configuration was demonstrated to achieve stable characteristics, supporting high-end wireless devices. In [2], a graphene-based antenna was discussed with conformal characteristics, allowing parallel support for Wi-Fi, 5G, and Wi-Fi for triband applications. A circular-ring monopole design with an optimized ground plane was introduced to achieve good impedance for ultra-wideband (UWB) applications [3]. In [4], circular patch antennas were designed and discussed to support specific bands, particularly the TV white space spectrum, allowing reliable communication. A complementary split-ring resonator was designed on a dielectric resonator, allowing penta-band operation for wireless networking [5].

In [6], a small, inverted L-shaped design was proposed for 5G operation, focusing on minimal structural complexity while supporting good radiation. A ring-based design optimized to obtain stable wideband performance was reported in [7] with the help of characteristic mode analysis. Ref. [8] introduces new hybrid design techniques to increase radiation efficiency in millimeter-wave short-range communication. A compact antenna with minimum thickness supports dual-band operation with circular polarization, which is useful for wireless devices. Their design mainly aims to keep the antenna miniaturized while still maintaining good radiation performance [9].

A circularly polarized antenna was discussed with reduced structure thickness and good axial ratio over its bands. Planar designs incorporating stubs have been investigated to achieve desired bands and impedance, as reported in [10]. A four-element antenna structure is combined with a complementary split-ring resonator, achieving better behavior in the X-band regime. Integrating resonator elements can significantly improve antenna characteristics, such as efficiency and signal quality [11]. In addition, different element antennas integrated with resonators have been discussed in X-band applications by regulating resonance behavior. Ref. [12] presents a nonuniform slot compact Vivaldi antenna configuration demonstrated to achieve ultra-wideband performance. Another slot-loaded circular monopole design for wider bandwidth and removing

* Corresponding author: Bokkisam Venkata Sai Sailaja (sailajabokkisam@gmail.com).

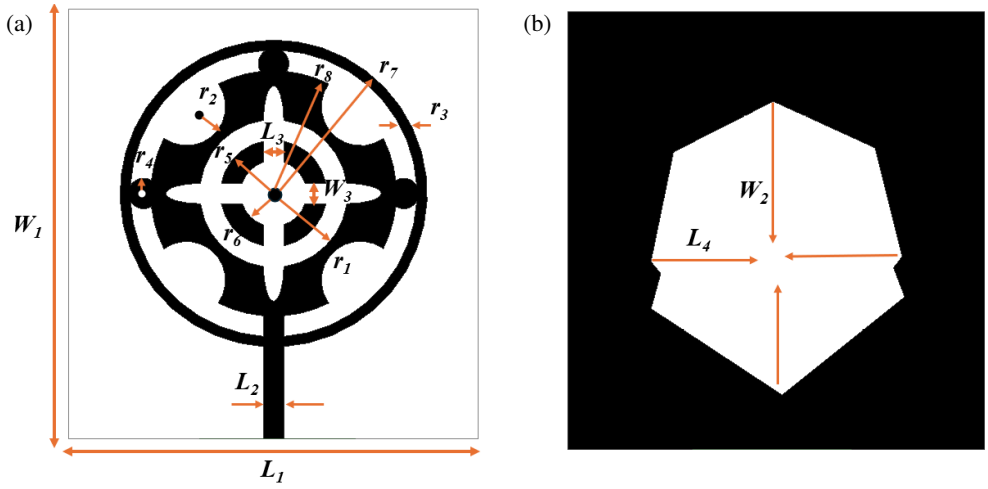

FIGURE 1. The schematic ultra-wideband circular slot Ring (UCSR) antenna with microstrip feed. (a) Front view. (b) Rear view.

unwanted frequencies is reported in [13]. Polymer-based substrate low-cost communication antennas are also used and reduce fabrication complexity, as discussed in [14], operating at 3.7 GHz. A metamaterial multilayered structure was developed to attain good gain and radiation for wireless networks, as given in [15]. An ultra-wideband design operating at 5G and microwave communication showcases strong interest in dual-mode operating designs, as demonstrated in [16]. To improve slot antenna performance behavior, ground-plane alteration and optimization for 5G bands are given in [17]. Ref. [18] presents metamaterial-based miniaturized antennas that continue to exhibit wider bandwidth behavior than conventional antennas for WLAN applications and Bluetooth systems. Resonator-inspired designs, such as artificial neural networks, have been introduced to tune the geometries for sub-6 GHz applications, as reported in [19]. In [20], an emerging millimeter-wave antenna for vehicular communication supports reliable data transmission. Ref. [21] discusses a super wideband antenna with controlled notch bands for future wireless applications.

In this work, a circular centric disc-structured ultra-wideband etched ring slot antenna is discussed. The circle-shaped, large ring with multiple etched slots has miniaturized the design by removing some portion of the structure. The UCSR antenna step configuration process is performed to validate the behaviour of the design. The UCSR antenna resonates at three operating bands, and its impedance bandwidth ranges from 2.71 to 12 GHz with good performance. The stable radiation patterns of the UCSR antenna in both E-plane and H-plane are presented at the three corresponding frequencies.

2. DESIGN DESCRIPTION

The circular compact cross-slotted structured design is outlined in Fig. 1. The design is built on an FR-4 substrate, with all parameters of length, width, and thickness as $40 \times 42 \times 1.6$ mm. FR-4 is a fairly used material, cost-effective, and easy to fabricate. On the left side of the figure, the main radiating element is visible. It is built with a simple circular patch. Another simple circular patch is etched at the center, having a radius of 15 mm. Inside the circular patch, a cross-shaped slot is etched, helpful in improving bandwidth. Near the slotted structure, four curved sections are developed, giving the design a symmetric appearance. A microstrip feed having a width of 2 mm is extended towards the patch and acts as a feed line. With the help of this feed line, the signal is carried from the source to the radiating patch. The circular patch and feed are integrated, and they are responsible for tuning the radiation and impedance matching. On the right side of the figure, the ground plane with an etched hexagonal structure is visible. Instead of going with a traditional full ground plane, a hexagonal structure is developed. In both images, the black portion depicts the copper material and the circular patch antenna with etched slots integrated together to make the antenna work effectively. Each characteristic of the design has a unique purpose, contributing to the design suitable for wireless communication requirements. The design of the UCSR antenna with full geometry is discussed in Fig. 1. The step configuration is demonstrated clearly in Fig. 2.

The FR4 substrate was modeled in ANSYS HFSS using the default material parameters ($\varepsilon_r = 4.4$, $\tan\delta = 0.02$), and a thickness of 1.6 mm is considered in this work. Fig. 2 shows the step-by-step configuration of the UCSR antenna design. In Fig. 2(a), a small, simple circular patch is developed. In Fig. 2(b), cross-shaped slots are created to widen impedance matching and coupling. Fig. 2(c) demonstrates a circular slot ring that provides current paths, generating multiple frequencies. Finally, in Fig. 2(d), the final UCSR antenna configuration is formed. This step configuration clearly shows how each structural updating leads to bandwidth improvement. Fig. 3 explains the fabricated UCSR antenna with a network analyzer. The compact geometry is fabricated perfectly according to the design specifications. This final UCSR antenna prototype showcases and confirms its suitability for ultra-wideband applications.

The prototype of the UCSR antenna is shown in Fig. 3. The operating frequency of the UCSR antenna is discussed with the following mathematical formulae [1–5]. The dimension values are discussed in Table 1. The ring loop circumference of the antenna is when an integer n (guided wavelength) fits the cir-

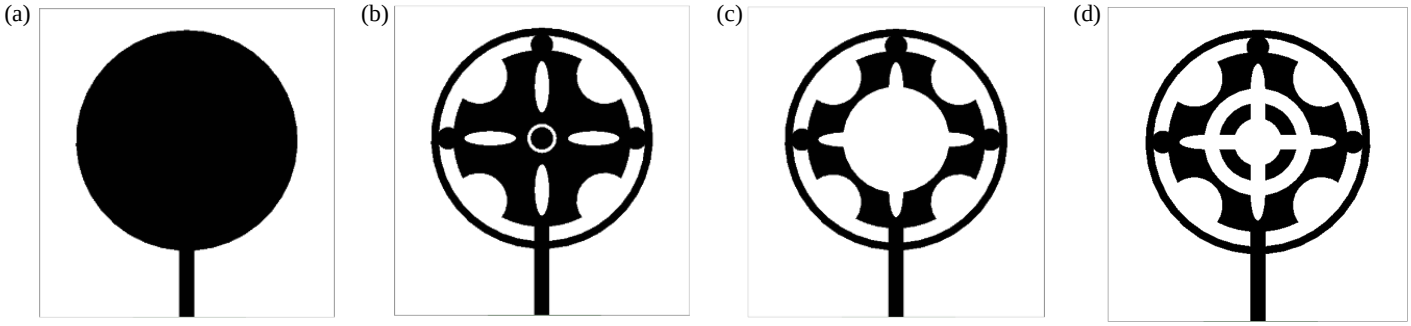

FIGURE 2. The step configuration process of the UCSR antenna illustrated in (a) Step configuration 1, (b) Step configuration 2, (c) Step configuration 3, (d) Step configuration 4.

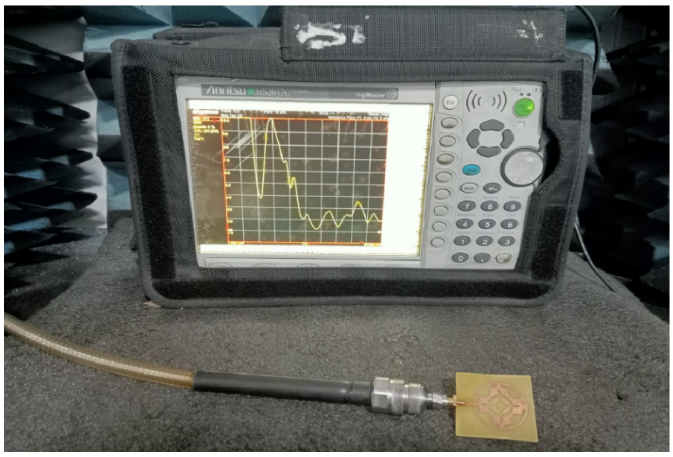

FIGURE 3. Prototype of the UCSR antenna with network analyzer.

cumference.

$$f_n = \frac{nc}{2\pi r_{eff}\sqrt{\varepsilon_{eff}}}; \quad n = 1, 2, \ldots \tag{1}$$

f_n: the nth resonant frequency of the circular ring, n: resonance mode number ($n = 1, 2, 3, \ldots$).

The approximation of the electrical path bounded by the inner radius and outer radius is given as

$$r_{eff} \approx \frac{r_{out} + r_{in}}{2} \tag{2}$$

R_{eff}: effective radius of the ring, r_{out}: outer radius of the circular slot, r_{in}: inner radius of the circular slot.

The narrow petal arms behave as a quarter-wave resonator.

$$f = \frac{c}{4L_{slot}\sqrt{\varepsilon_{eff}}} \tag{3}$$

f: resonant frequency of the slot arm, L_{slot}: effective length of the slot arm.

The resonance frequency at TM_{01} for a circular central disc-like structure.

$$f_{01} \approx \frac{X_{01}c}{2\pi a\sqrt{\varepsilon_{eff}}} \tag{4}$$

X_{01} — 2.4048, a — effective radius, c — speed of light.

TABLE 1. The values of the UCSR antenna.

Geometry	Value (mm)	Geometry	Value (mm)
L_1	42	r_1	7.2
W_1	40	r_2	3.81
L_2	2	r_3	14
L_3	2	r_4	1.5
W_2	28	r_5	5.2
W_3	2	r_6	3.2
L_4	24	r_7	15
		r_8	12

The effective permittivity of the antenna is approximated by

$$\varepsilon_{eff} \approx \frac{\varepsilon_r + 1}{2} + \frac{\varepsilon_r - 1}{2}\frac{1}{\sqrt{1 + 12h/W}} \tag{5}$$

h — substrate thickness, W — width of the patch.

3. RESULTS AND DISCUSSION

The simulated (S_{11}) evaluation for the four-step configuration of the UCSR antenna is given in Fig. 4. The operating band increases with each step for fine refinement. In the first configuration, the frequency is not well resonated and attains a minimum bandwidth. The design goes through extra slots and structural changes; consequent steps widen impedance matching. The final step-configuration is shown in Fig. 4. Step 4 shows four operating frequencies with better S_{11} values, indicating good bandwidth. This illustrates that each update leads to the overall multiband behaviour of the UCSR antenna. The performance analysis of the voltage standing wave ratio (VSWR) is discussed with simulated and measured values in Fig. 5. There is close overlap, which validates the reliability of the design and confirms the efficient power transfer and minimal reflection. Fig. 6(a) shows the top view of the circular slot ring with a central disc structure; similarly, the bottom view in Fig. 6(b) represents the ground with an etched hexagon. To sum up, the results agree with steady performance from the basic structure to a well-structured antenna.

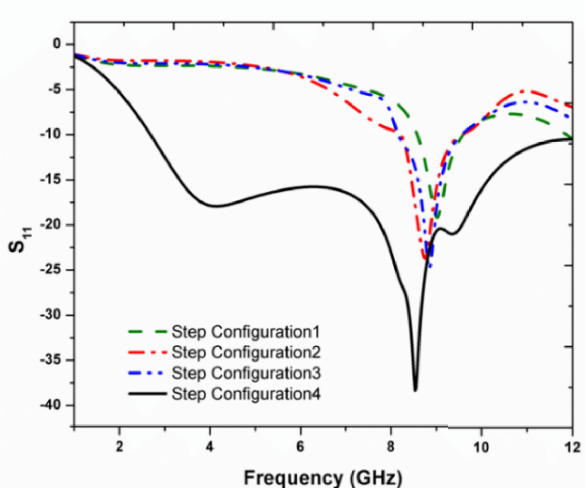

FIGURE 4. Illustrate the S_{11} response of the UCSR antenna observed during each step configuration process.

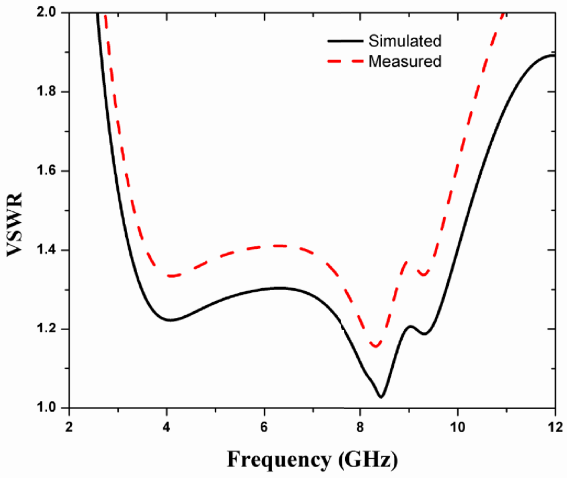

FIGURE 5. VSWR of UCSR antenna across wide operating frequency.

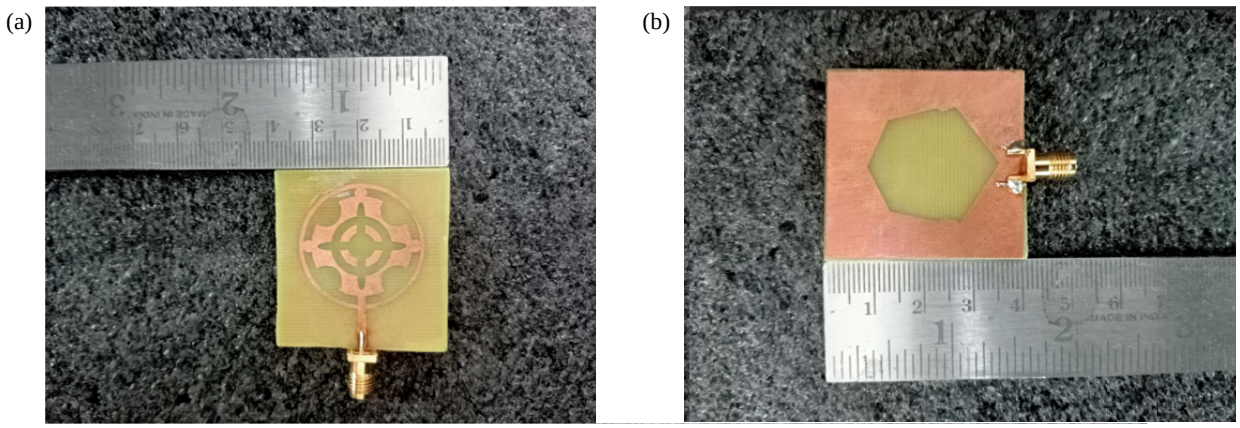

FIGURE 6. Fabricated design of UCSR antenna, (a) top view, (b) bottom view.

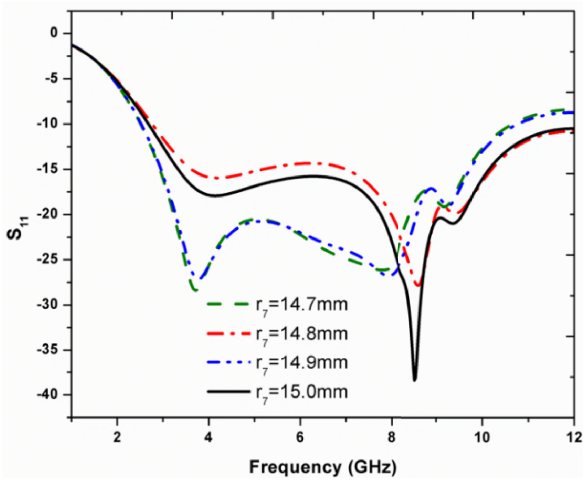

FIGURE 7. S_{11} variation of the UCSR antenna as the parameter r_7 changes from 14.7 mm to 15.0 mm.

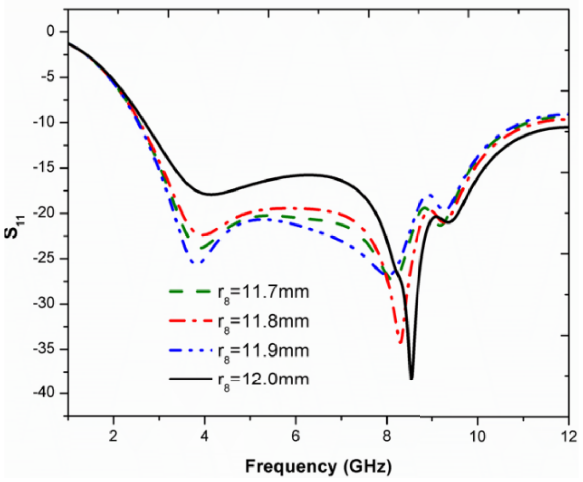

FIGURE 8. S_{11} variation of the UCSR antenna as the parameter r_8 changes from 11.7 mm to 12.0 mm.

Figure 7 presents the variation of the S_{11} characteristics with different values of the outer ring radius (r_7). As the radius varies from 14.7 mm to 15.0 mm, only a slight shift in the resonant peaks is noticed. It indicates that small changes in r_7 mainly fine-tune the resonance. At $r_7 = 15$ mm, the best resonance is achieved. Similarly, Fig. 8 explains the impact of tun-

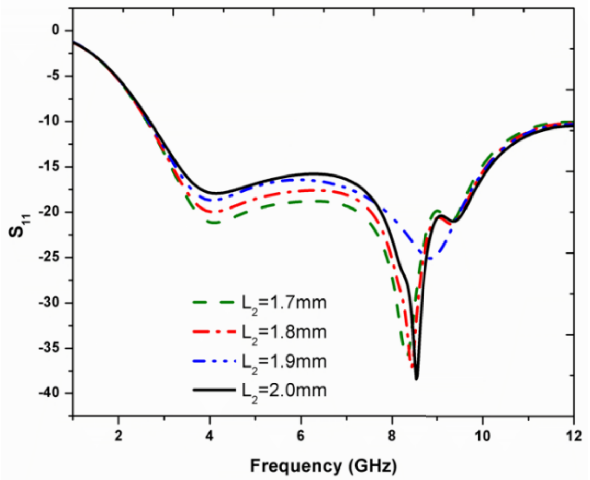

FIGURE 9. S_{11} variation of the UCSR antenna as the parameter L_2 changes from 1.7 mm to 2.0 mm.

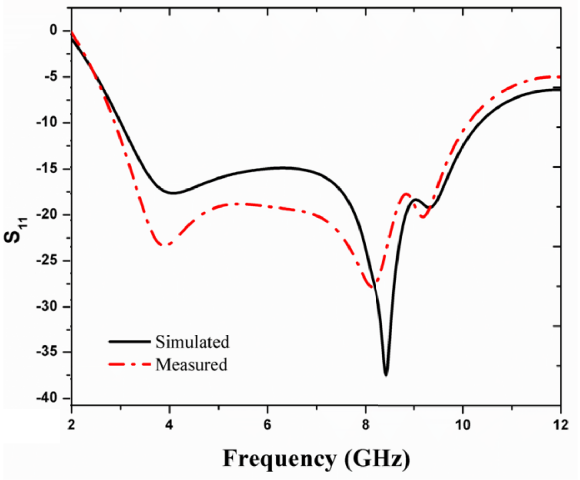

FIGURE 10. The comparison between the simulated and measured S_{11} variations of the UCSR antenna.

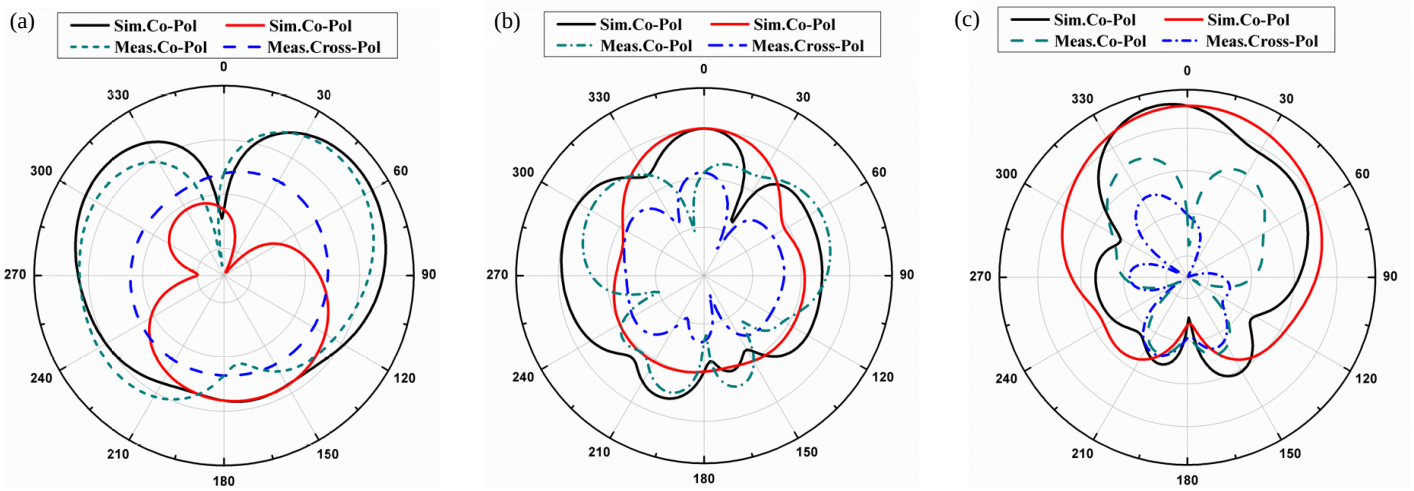

FIGURE 11. The radiation characteristics of the UCSR antenna at different frequencies: (a) 4.13 GHz, (b) 8.53 GHz, and (c) 9.09 GHz, respectively.

ing r_8 from 11.7 mm to 12 mm. This parameter (r_8) controls the effective current path, which changes the equivalent circuit RLC values of the antenna. Due to this, minute variations in R_8 modify the bandwidth and impedance matching rather than generating frequencies. The effect of the L_2 is studied from 1.7 mm to 2 mm, as shown in Fig. 9. L_2 directly influences the input impedance between feed and radiator. Therefore, choosing the correct L_2 value achieves balanced performance over the bands. The parametric results of r_7, r_8, and L_2 are discussed in Fig. 7, Fig. 8, and Fig. 9, respectively. These results confirm that each parameter plays a unique role in varying the antenna response. By considering all these parameters, the antenna works exceptionally well. The measured S_{11} response is shown in Fig. 10. The two lines are very close to each other, confirming that the fabrication validates both the design method and the fabrication accuracy. Finally, the radiation plots of the UCSR antenna are discussed in Fig. 11 by analyzing co-pol and cross-pol at 4.13 GHz, 8.53 GHz, and 9.09 GHz. The patterns remain omnidirectional and almost consistent across all the bands.

In fabricated antennas, a good match between simulation and measurement is observed due to most of the experimental parameters. The slight variation between simulated and experimental values of VSWR and S_{11} responses is due to fabrication tolerances, dielectric properties of the material, and soldering effects.

Figure 12 explains the comparison of radiation efficiency between simulated and measured values across frequency. This comparison helps to verify how effectively the proposed UCSR antenna achieves better performance. The radiation efficiency is stable over the 2.71–12 GHz range, with good performance noticed near the main frequencies. This states that the UCSR design maintains good radiation over the band. The measured results steadily follow the simulated values, with a minimal variation between them. This agreement showcases the accuracy of the fabrication process and design analysis. The obtained values are approximately 75% to 85% across the 2.71–12 GHz band, while the measured values are between 72% and 82%. The achieved group delay remains almost consistent overall in frequency, with a very minimal variation of less than

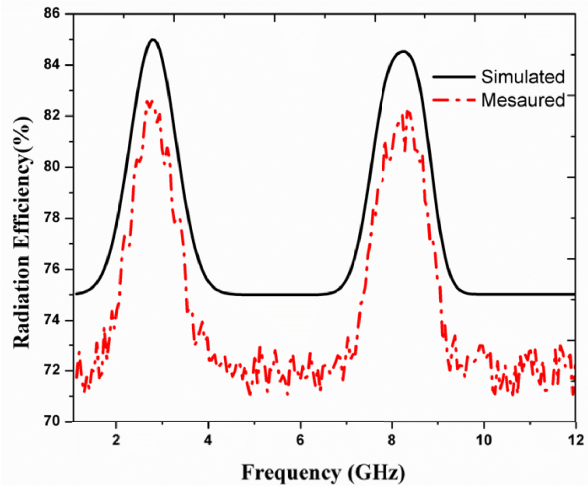

FIGURE 12. Comparison of radiation efficiency (sim and meas) values across frequency.

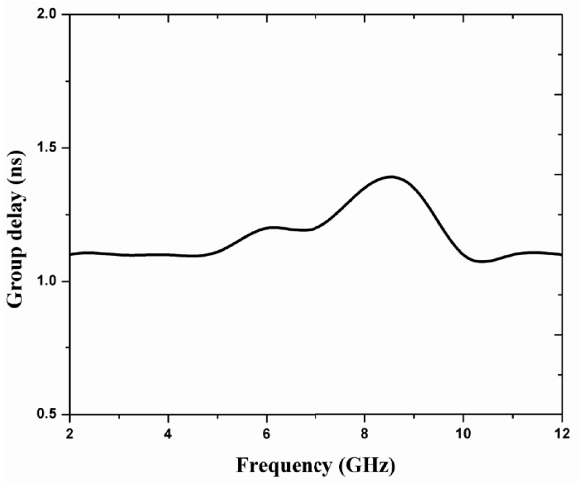

FIGURE 13. Performance of group delay UCSR antenna.

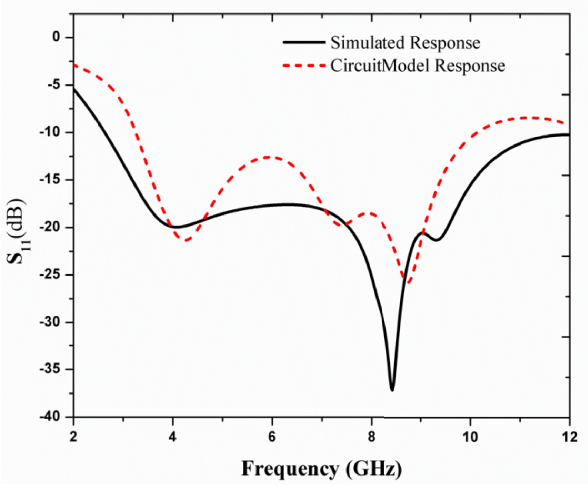

FIGURE 14. The S_{11} response vs circuit model response of antenna element.

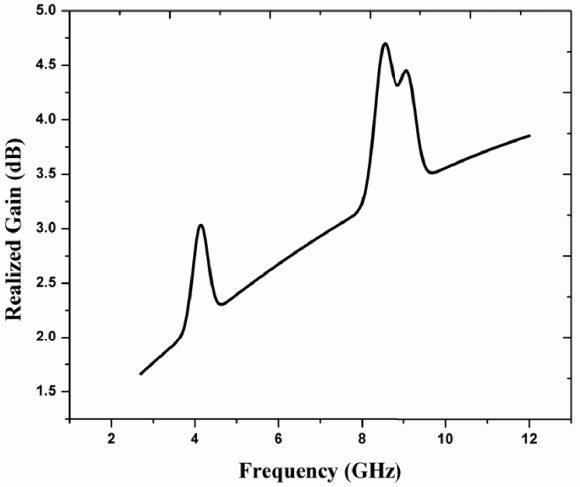

FIGURE 15. The average realized gain of the UCSR antenna.

0.3 ns. It indicates that uniform propagation across the frequencies is experienced by the signal.

The obtained group delay line is mostly flat and continuous, maintaining an average between 1 ns and 1.4 ns, exhibiting stable phase response. A steady group delay is necessary for achieving signal quality in UWB designs. Due to this minor variation transmitted, such a minor variation ensures that transmissions remain almost unchanged during propagation with minimal distortion. This makes the design appropriate for better speed data transmission. Fig. 13 illustrates the group delay performance of the UCSR antenna. The plot clearly confirms the stable and reliable time-domain behaviour of the proposed design.

Figure 14 provides the simulated S_{11} (solid line) with the RLC model (dashed line) of the UCSR antenna over 2.71–12 GHz. The close agreement between the two lines indicates that the RLC model finally analyzes the antenna behaviour. The two curves exhibit nearly identical values in impedance variation, confirming that the circuit effectively presents multiband characteristics. This explains the reliability of the analytical modeling performed for the design. The plot (Fig. 14) compares full-wave S_{11} responses with circuit model S_{11} discussed in detail.

The proposed antenna exhibits peak realized gain values of 3.03 dBi at 4.13 GHz, 4.70 dBi at 8.53 GHz, and 4.45 dBi at 9.09 GHz, corresponding to the three resonance frequencies within the operating band, as shown in Fig. 15. These gain values indicate that the antenna radiates effectively without compromising for the best performance. The average realized gain over the entire frequency band is given below. This average value helps in analyzing the consistency of the antenna in terms of radiation. The UCSR antenna achieves an average realized gain of 3.11 dBi across the UWB, producing stable radiation. This achievement confirms that the antenna performance does not degrade drastically within the working range.

Figure 16 exhibits the surface current distributions at eight different angles: 0°, 15°, 30°, 45°, 60°, 75°, 90°, and 120°. These currents support how different parts of the design con-

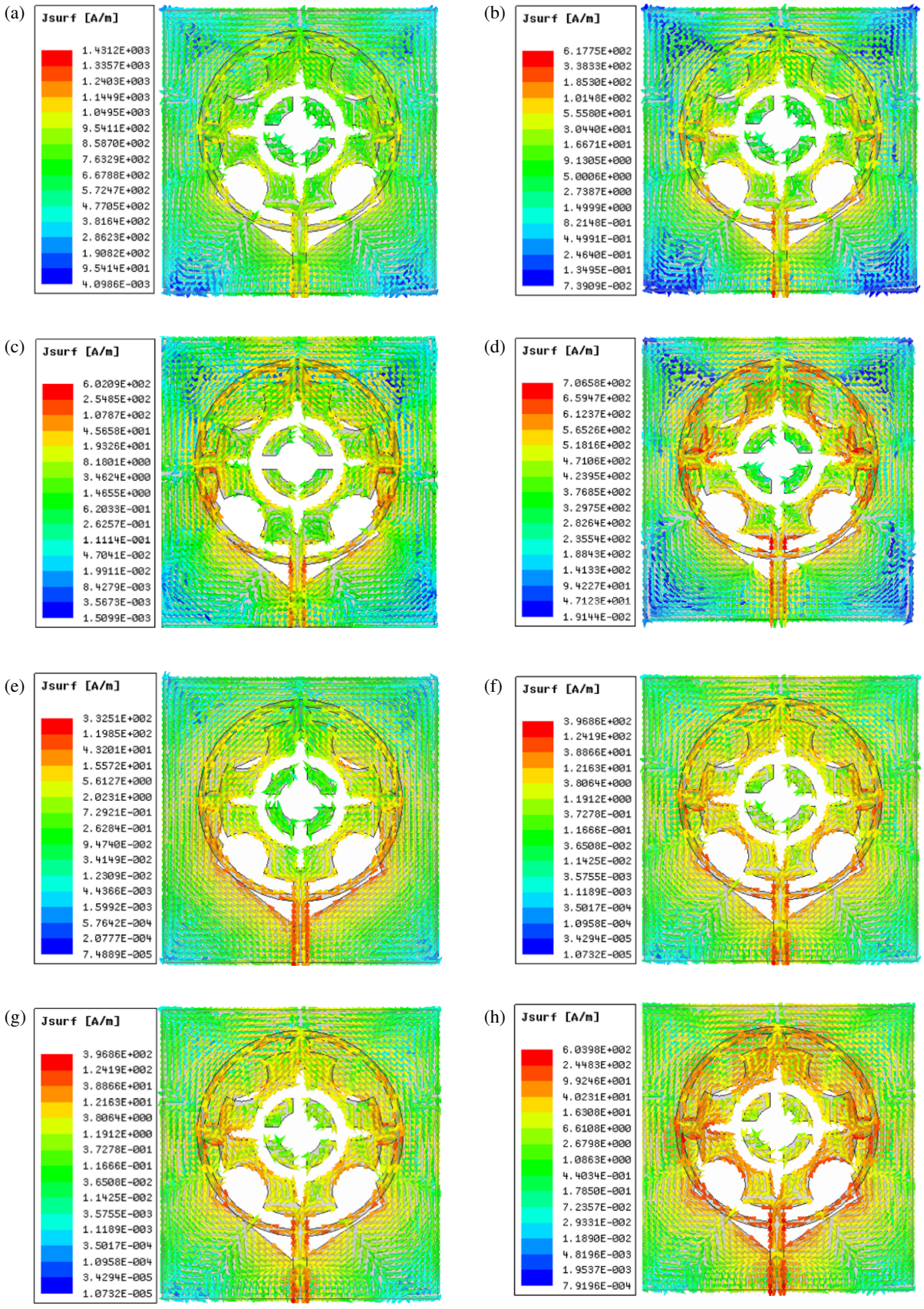

FIGURE 16. The UCSR antenna model presenting current distributions at eight different angles from 0°, 15°, 30°, 45°, 60°, 75°, 90°, and 120°.

TABLE 2. Comparison of the UCSR antenna with previous works published.

Ref.	Operating frequency (GHz)	Reflection coefficient (dB)	Bandwidth	Gain (dBi)	Application
7	3.03–11.75	−32	50%	5	UWB wireless communication systems
9	3.20–6 6.58–6.73	−25 −30	61%	4	Wireless applications
10	3.32–5.02 6.27–11.35 13.13–18.24	−18 −25 −20	121%	4.5	X-band Ku band
13	2.69–4.36 5.5–7.14 12.26–14.44 17.39–19.60	−18 −22 −28 −20	110%	4	Wireless Applications.
21	5.5–7.3 12.05–14.46 17.71–19.5	−20 −30 −22	166%	5	Wireless applications
This work	(2.71–12) 4.13 8.53 9.09	−17.9 −38 −20	128.7%	3.03 4.75 4.46	5G, UWB, RADAR

tribute to radiation at different orientations. The comparison of the UCSR antenna design with published works is produced in Table 2.

The UCSR antenna design attains an operating bandwidth of 2.71–12 GHz, with resonant frequencies at 4.13 GHz ($S_{11} = -17.9$ dB), 8.53 GHz ($S_{11} = -38$dB), and 9.09 GHz ($S_{11} = -20$ dB). These deep return loss values confirm good impedance matching at the desired bands. These values illustrate immense radiation strength for practical modern wireless communication systems. The proposed design operates for UWB, radar, and 5G applications.

4. CONCLUSION

In this paper, a compact multiband UCSR antenna is presented for UWB wireless communication. The designed antenna exhibits reasonable return loss at three resonant frequencies (4.13 GHz, 8.53 GHz, and 9.09 GHz), which indicate the good impedance matching and stable radiation of radiator currents. It also has a wide impedance bandwidth ranging from 2.71 GHz to 12 GHz, which is more suitable for high data-rate transmission of UWB systems. The circular slots, ring structures, and defected ground plane lead to multiband behavior and high gain, approximately 5 dBi, as well as compact dimensions on a low-cost FR-4 substrate. Because of the ultra-bandwidth characteristics, stable radiation patterns, and triple-band operation, the designed UCSR antenna is a suitable candidate for 5G communication, radar systems, military devices, and other UWB applications. Overall, the proposed design can serve as a simple and low-cost alternative solution to achieve effective performance for integrated wireless communication systems in the future.

REFERENCES

[1] Sundaravadivel, P., M. R. Raja, C. Annadurai, and D. R. Kumar, "A novel moon-shaped flexible four-element co-planar antenna for 5G applications," *Optical and Quantum Electronics*, Vol. 56, No. 10, 1612, Sep. 2024.

[2] Ye, D., H. Zu, Z. Hu, Y. Xin, J. Guo, R. Song, and D. He, "Flexible and compact tri-band graphene antenna for conformal Wi-Fi/WiMAX/5G applications," *IEEE Transactions on Circuits and Systems II: Express Briefs*, Vol. 71, No. 3, 1086–1090, Mar. 2024.

[3] Ali, S. Z., I. E. Khuda, K. Raza, and M. Ebrahim, "Measurement engineering to design a truncated ground plane compact circular ring monopole patch antenna for ultra wideband applications," *Wireless Personal Communications*, Vol. 124, No. 2, 1317–1336, 2022.

[4] Sharma, R., N. S. Raghava, and A. De, "Design and analysis of circular microstrip patch antenna for white space TV band application," *Wireless Personal Communications*, Vol. 126, No. 4, 3333–3344, 2022.

[5] Rath, S., G. Palai, and K. L. Sheeja, "A penta-band CSRR loaded dielectric resonator antenna for X-Band, W-LAN, Wi-Fi 6, and Wi-Max applications," *Optical and Quantum Electronics*, Vol. 56, No. 8, 1374, 2024.

[6] Kulkarni, N., R. M. Linus, and N. B. Bahadure, "A small wideband inverted L-shaped flexible antenna for sub-6 GHz 5G applications," *AEU — International Journal of Electronics and Communications*, Vol. 159, 154479, Feb. 2023.

[7] Xiang, Z., Z. Wang, C. Li, and R. You, "Design of UWB monopole antenna with ring structure based on characteristic mode theory," *Progress In Electromagnetics Research C*, Vol. 158, 225–234, 2025.

[8] Islam, T., D. Hussain, F. N. Alsunaydih, F. Alsaleem, and K. Alhassoon, "Designing a novel hybrid technique based on enhanced performance wideband millimeter-wave antenna for

short-range communication," *Sensors*, Vol. 24, No. 10, 3219, May 2024.

[9] Hu, M., Y. Li, Y. Zhang, P. Wu, and H. Wang, "Ultrathin dual-band circularly polarized antenna," *IEEE Antennas and Wireless Propagation Letters*, Vol. 23, No. 3, 930–934, Mar. 2024.

[10] Lakshmaiah, Y. V. and B. Roy, "Planar monopole antenna based on surface roughness and stub loaded with notch controlling characteristics," *Transactions on Electrical and Electronic Materials*, Vol. 24, No. 6, 502–510, 2023.

[11] Sasikumar, J. and V. Koushick, "Performance analysis of complementary split ring resonator with improved four element antenna for X band wireless applications," *Progress In Electromagnetics Research M*, Vol. 130, 95–102, 2024.

[12] Saleh, S., T. Saeidi, N. Timmons, B. Alali, F. Razzaz, and A. A. Althuwayb, "Compact ultra-wide band two element vivaldi non-uniform slot MIMO antenna for body-centric applications," *Results in Engineering*, Vol. 24, 102839, 2024.

[13] Lakshmaiah, Y. V. and B. Roy, "A circular monopole antenna for bandwidth enhancement using cylinder slots with triple band notch characteristics," *International Journal of Communication Systems*, Vol. 36, No. 7, e5453, 2023.

[14] Lee, Y., S.-H. Choi, B.-H. Lee, J.-Y. Lee, and J. H. Kim, "LCP-based low-cost base station antenna for 3.7 GHz 5G band," *Journal of Electromagnetic Engineering and Science*, Vol. 24, No. 3, 276–284, May 2024.

[15] Fathipour, M. and L. Asadpor, "Design and fabrication of a multilayer metamaterial antenna with high-gain and good radiation patterns for WiFi and WiMAX applications," *IET Communications*, Vol. 17, No. 4, 448–459, 2023.

[16] Yadav, S. V., M. V. Yadav, V. Singh, K. P. Bhati, D. Yadav, T. Ali, and S. B. S, "Miniaturized UWB antenna design for 5G and space-based microwave applications," *Results in Engineering*, Vol. 27, 105592, 2025.

[17] Gaber, M. A., M. El-Aasser, A. Yahia, and N. Gad, "Characteristic modes of a slot antenna design based on defected ground structure for 5G applications," *Scientific Reports*, Vol. 13, No. 1, 15327, 2023.

[18] Chen, G., C. Guo, J. Xue, Z. Wang, and M. Pang, "Miniaturized metamaterial ultra-wideband antenna for WLAN and Bluetooth applications," *Progress In Electromagnetics Research C*, Vol. 132, 117–127, 2023.

[19] Shobana, M., "CSRR inspired antenna using artificial neural network for sub 6 GHz 5G applications," *Alexandria Engineering Journal*, Vol. 77, 351–367, 2023.

[20] Munir, M. E., M. M. Nasralla, and H. Farman, "Design and development of super-compact millimeter wave antenna for future 5G vehicular applications," in *2024 IEEE 100th Vehicular Technology Conference (VTC2024-Fall)*, 1–8, Washington, DC, USA, 204.

[21] Lakshmaiah, Y. V. and D. B. Roy, "Super wideband with band rejection characteristics circular patch monopole antenna for 5G and beyond," *Physica Scripta*, Vol. 98, No. 9, 095513, 2023.